J Mater Sci (2008) 43:4363–4369
DOI 10.1007/s10853-008-2556-7

Polyacrylonitrile/vapor grown carbon nanofiber composite films

Huina Guo · Asif Rasheed · Marilyn L. Minus · Satish Kumar

Received: 15 October 2007 / Accepted: 13 February 2008 / Published online: 18 April 2008

Abstract Polyacrylonitrile (PAN)/vapor grown carbon nanofiber (VGCNF) composite films were processed from *N*, *N*-dimethylformamide (DMF) at various nanofiber loadings: 5, 10, 20, 40, 60, 80, and 90 wt%. Tensile, dynamic mechanical, electrical, structural, and morphological properties of these composite films were studied. Enhancement in tensile properties was observed in composites with nanofiber loading up to 40 wt%. The storage modulus of PAN increased upon incorporation of nanofiber particularly above the glass transition temperature. The tan δ peak broadens and shifts to higher temperatures with the addition of VGCNF. The activation energy for PAN molecular motion was higher than that in the control PAN film. The electrical conductivity of composite films increased with increasing nanofiber loading and exhibited a percolation at 3.1 vol%. Scanning electron microscopy (SEM) indicated PAN coated nanofibers in the composite film.

Introduction

Vapor grown carbon nanofibers (VGCNFs) were developed in the 1980s [1–4]. They differ from other types of carbon fiber in their method of production and their microstructure. Uchida et al. [5] studied the microstructure of nanofibers by transmission electron microscopy. A truncated cone microstructure of VGCNFs was observed with outer and inner diameters of 60 and 25 nm, respectively. The graphite sheets in nanofibers were found to be oriented at an average angle of about 15° with respect to the fiber axis. VGCNFs have been incorporated into a variety of polymers in the form of films and fibers, such as epoxy [6–8] polyethylene [9], polypropylene [10–15] polycarbonate [13, 14, 16–20] polystyrene [21] acrylonitrile-butadiene-styrene (ABS) [22], nylon [23, 24], poly(phenylene sulfide) [7], phenylethynyl terminated polyimide [25], poly(methyl methacrylate) [6, 26], poly(ethylene terephthalate) (PET) [27], and poly(p-phenylene benzobisthiazole) (PBZT) [28].

Property improvements in polymer with incorporation of VGCNF include electrical properties [8, 11, 14, 20] mechanical properties [10, 12, 14] thermal stability [10, 20], as well as crystallization rate [10]. Rheological properties of VGCNF-reinforced nanocomposites have also been studied [9, 11, 13, 17]. PP/VGCNF composites were reported to exhibit an electrical conductivity percolation threshold of 9–18 wt% [11]. The percolation threshold of PC/VGCNF composites was reported at 6.3 wt% [20]. PP/VGCNF composites with 15 wt% fiber loading showed 90% enhancement in Young's modulus over the control polymer [14]. In another study, a 60% increase in Young's modulus and a 35% reduction in the thermal expansion coefficient were observed for PP/VGCNF bulk composites with 5 vol% fiber loading [10]. The storage modulus at room temperature increased by 350% for PP/VGCNF composites containing 60 wt% VGCNF as compared to the control PP [12]. PAN/VGCNF composite fibers with significant property improvements have been reported [29].

H. Guo · A. Rasheed · M. L. Minus · S. Kumar (✉)
School of Polymer, Textile and Fiber Engineering,
Georgia Institute of Technology, Atlanta, USA
e-mail: Satish.Kumar@ptfe.gatech.edu

Present Address:
A. Rasheed
Department of Chemistry, University of Wisconsin,
Whitewater, WI, USA
e-mail: rasheeda@uww.edu

In this study, composite films of polyacrylonitrile (PAN) and VGCNF were processed and characterized. VGCNF was varied from 5 wt% to as high as 90 wt% in the composite. PAN was chosen due to its commercial importance as a predominant carbon precursor. The films were characterized for their mechanical, electrical, structural, and morphological properties. The film thickness was typically 25 μm.

Experimental

Materials

PAN (molecular weight = 100,000 g/mol) obtained from Exlan Co. (Japan) and dimethylformamide (DMF) supplied by Sigma-Aldrich were used as received. VGCNF (Grade PR-24-HT) was obtained from Applied Sciences Inc. (Cedarville, OH).

Preparation of PAN/VGCNF composite films

Dried VGCNFs were dispersed in DMF by sonication in a sonic bath (Cole-Parmer 8891R-DTH, 80 W, 43 kHz) for 48 h. Homogenous dispersion of VGCNF in DMF was confirmed by optical microscopy. Dried PAN was dissolved separately in DMF, and the PAN/DMF solution was subsequently added to the VGCNF dispersion. The resultant PAN/VGCNF/DMF dispersion was stirred and excess solvent was evaporated to obtain the desired volume. The PAN/VGCNF/DMF dispersion was cast on the glass substrate to form the film in the vacuum oven at 80 °C. The composite film was peeled off the glass substrate and further dried in vacuum oven at 80 °C for 3 days. The composite films with various loadings of VGCNFs (5, 10, 20, 40, 60, 80, 90 wt% CNFs) were prepared using the same procedure.

Characterization of composite films

An RSA III instrument manufactured by Rheometrics Scientific was used to measure the tensile and dynamic mechanical properties. The gauge length, film width, and strain rate for the tensile tests were 20 mm, 2 mm, and 10%/min, respectively. Dynamic mechanical measurement was carried out at the testing frequencies of 0.1, 1, 5, and 10 Hz, and a temperature increment of 1 °C/min. SEM imaging of composite films was done on gold coated films using a Leo 1530 Scanning Electron Microscope. In-plane dc electrical conductivity was measured by a four-probe method. X-ray diffraction studies were conducted on Rigaku R-AXIS IV^{++} equipped with an image plate. The CuKα radiation monochromatized by a confocal optics system (wavelength = 0.15418 nm) was used and data analysis was done using jade software.

Results and discussion

The tensile properties of PAN/VGCNF composites with various nanofiber loadings are given in Table 1. The initial modulus of the composite film with 5% VGCNF loading was about 20% higher than the modulus of control PAN film, while the tensile strength of this composite film was 50% higher than that of control PAN film. Further enhancement in tensile properties was not observed upon increased VGCNF loading. VGCNF loading higher than 40% in the composite film yielded tensile properties lower than that for the control PAN film. The gradual decrease in tensile strength in composites films with increased nanofiber content could be attributed to the presence of defects such as voids as evident by the difference in experimental and calculated densities of the composites. The observed and theoretical density values are listed in Table 2. The measured density of the composite films was lower than the calculated density for all the composites except for the film with 5% VGCNF loading. From the difference in theoretical and observed densities, void fraction, ϕ, in the composite films can be estimated as,

$$\phi = \frac{\rho_{\text{theo}} - \rho_{\text{obs}}}{\rho_{\text{theo}}}$$

where ρ_{theo} is the calculated density and ρ_{obs} is the observed density of the composite films. The estimated values of void content in the composite films are given in Table 2. The detrimental effects of voids on composite properties are well known [30–32]. Figure 1 shows the plot of void content and tensile strength as a function of nanofiber loading, which clearly indicates a decrease in tensile strength of the composite with increasing void content. The inset of Fig. 1 shows the plot between tensile strength and void content indicating a correlation between the two. However, to fully realize the potential of the nanofiber in the composite, methods need to be developed to eliminate the presence of voids.

Table 1 Mechanical properties of control PAN and PAN/VGCNF composite films

VGCNF loading (wt%)	Tensile modulus (GPa)	Tensile strength (MPa)	Elongation (%)
0	3.7 ± 0.4	53 ± 9	3.2 ± 1.5
5	4.4 ± 0.3	80 ± 6	5.5 ± 1.6
10	4.1 ± 0.3	73 ± 6	3.7 ± 0.5
20	4.0 ± 0.2	59 ± 3	2.5 ± 0.3
40	5.4 ± 0.5	57 ± 9	1.4 ± 0.3
60	3.2 ± 1.2	19 ± 6	0.8 ± 0.2
80	1.6 ± 0.7	12 ± 4	1.5 ± 0.6
90	1.1 ± 0.1	6 ± 1	1.2 ± 0.4

Table 2 Electrical conductivity and density of control PAN and PAN/VGCNF composite films

VGCNF loading (wt%)	VGCNF loading (vol%)	Conductivity (S/m)	Observed density (g/cm^3)	Theoretical density[a] (g/cm^3)	Void content (%)
0	0	–	1.15 ± 0.06	1.18	–
5	3.1	0.7 ± 0.6	1.22 ± 0.07	1.20	–
10	6.3	35.2 ± 11.7	0.91 ± 0.09	1.23	26
20	13.1	88.8 ± 18.6	0.66 ± 0.05	1.28	48
40	28.7	(8.8 ± 0.2) × 10^2	0.81 ± 0.01	1.40	42
60	47.6	(1.06 ± 0.04) × 10^3	0.73 ± 0.06	1.55	53
80	70.8	(1.57 ± 0.06) × 10^3	0.51 ± 0.06	1.72	70
90	84.5	(1.67 ± 0.08) × 10^3	0.50 ± 0.09	1.83	73

[a] Theoretical density of the composite films is calculated using the following equation: $\rho_c = V_f\,(\rho_f - \rho_m) + \rho_m$

where ρ_c is the density of the composite film, V_f is the volume fraction of VGCNF, ρ_f is the density of VGCNF (1.95 g/cm^3), and ρ_m is the density of PAN (1.18 g/cm^3)

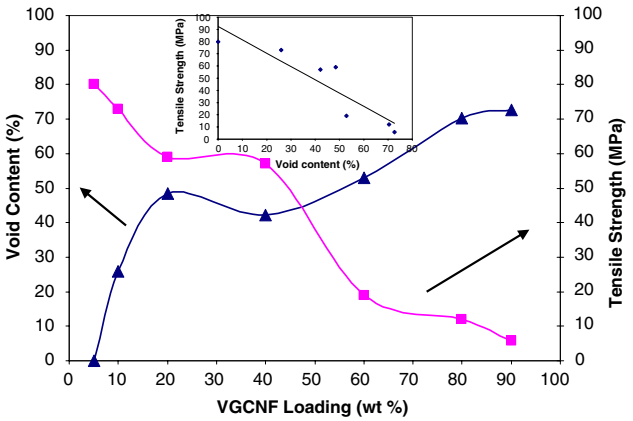

Fig. 1 Tensile strength and void content of composite films as a function of VGCNF loading. Inset is the plot of tensile strength versus void content (correlation coefficient = 0.903)

The theoretical modulus of the composite films can be predicted using Halpin-Tsai equation [33] given as,

$$E_C = \frac{3}{8}E_{11} + \frac{5}{8}E_{22} \tag{1}$$

$$E_{11} = \frac{1 + 2(l_{nf}/d_{nf})\eta_L V_{nf}}{1 - \eta_L V_{nf}} E_m \tag{2}$$

$$E_{22} = \frac{1 + 2\eta_T V_{nf}}{1 - \eta_T V_{nf}} E_m \tag{3}$$

$$\eta_L = \frac{E_{nf}/E_m - 1}{E_{nf}/E_m + 2(l_{nf}/d_{nf})} \tag{4}$$

$$\eta_T = \frac{E_{nf}/E_m - 1}{E_{nf}/E_m + 2} \tag{5}$$

where l_{nf} and d_{nf} are the length and diameter of the nanofiber, respectively, and E_{nf} and E_m are the moduli of the nanofiber and the polymer matrix, respectively. The parameters used in the Halpin-Tsai equation are listed in Table 3. The theoretical specific moduli calculated using a VGCNF modulus of 50 GPa [5] for various nanofiber lengths and the experimental specific moduli are plotted as a function of VGCNF loading of up to 40% (Fig. 2). The predicted modulus of the composite film increased significantly with increasing nanofiber length from 200 nm up to 10 μm. However, further increase in nanofiber length to 100 μm did not result in significant increase in the calculated modulus. At 5 wt% VGCNF loading, the theoretical modulus of the film corresponding to the nanofiber length of 10 μm agrees well with the experimental value. The experimental specific moduli were higher than the theoretical one for the composite films containing 10 and 20% nanofiber. The theoretical modulus for the composite films was calculated based on the VGCNF morphology where all graphite layers were oriented at 15° to the nanofiber axis. However, two types of morphologies in VGCNF were observed: single-layer nanofiber and double-layer

Table 3 Parameters used in Halpin-Tsai equation

Modulus of VGCNF, E_{nf} (GPa)	Modulus of PAN, E_m (GPa)	Length of VGCNF, l_{nf} (μm)	Diameter of VGCNF, d_{nf} (nm)	Density of VGCNF, ρ_{nf} (g/cm^3)
50 and 72 [5]	3.7	0.2–100	60	1.95 [1]

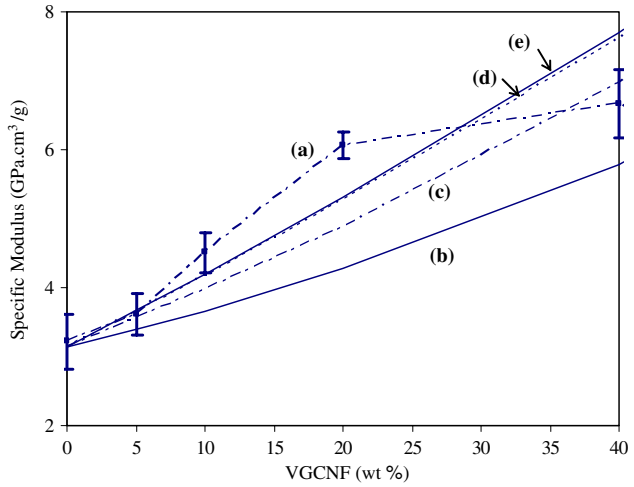

Fig. 2 Experimental and theoretical specific modulus of various PAN/VGCNF composite films assuming the modulus of VGCNF to be 50 GPa. (**a**) Experimental modulus, (**b**) theoretical modulus assuming VGCNF length to be 0.2 μm, (**c**) 1 μm, (**d**) 10 μm, and (**e**) 100 μm

nanofiber [5]. The graphite layers in the double-layer nanofiber were highly oriented in a second outer layer resulting in higher modulus [5]. Due to the existence of the higher orientation graphitic sheet in outer layer, the mechanical properties of double-layer CNF were higher than those of the single-layer CNF. For the double-layer VGCNF, the modulus was calculated to be 72 GPa [5]. Using this modulus, the theoretical specific modulus of the composite films for various nanofiber lengths were calculated using the Halpin-Tsai equation and plotted as a function of VGCNF loading (up to 40%) in the composite films (Fig. 3). The experimental specific moduli agree well

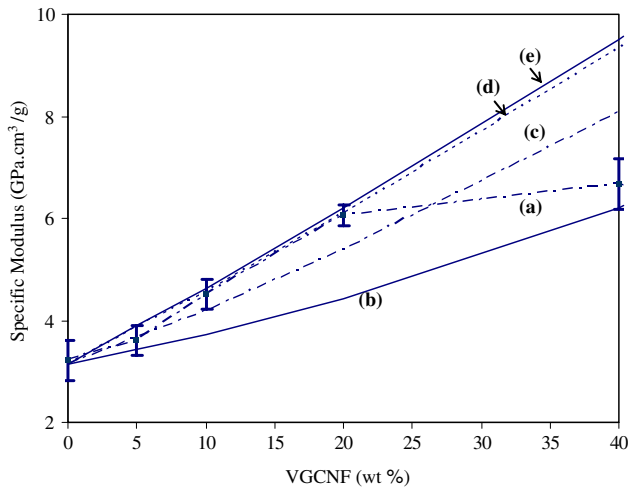

Fig. 3 Experimental and theoretical specific modulus of various PAN/VGCNF composite films assuming the modulus of VGCNF to be 72 GPa. (**a**) Experimental modulus, (**b**) theoretical modulus assuming VGCNF length to be 0.2 μm, (**c**) 1 μm, (**d**) 10 μm, and (**e**) 100 μm

with the theoretical one for the composite films with VGCNF loading as high as 20%. At a VGCNF loading of 40% or more, the experimental modulus of the composite films was significantly lower than the predicted value. For polypropylene/carbon nanofiber composites, Hine et al. [10] observed enhancement in Young's modulus of the composites. The experimental modulus agreed well with the model for composites containing nanofibers up to 10 wt% in polypropylene matrix. The measured modulus at a higher nanofiber loading (20 wt%) was significantly lower than the predicted value. Ogasawara et al. [25] compared their experimentally measured tensile modulus for VGCF/phenylethnyl terminated polyimide composites with the model. The data agreed well with the model when the elastic modulus of carbon nanofibers was 20 GPa. This observation was attributed to the weak bonding between the nanofiber and the polymer resulting in the sliding at the interface and poor stress transfer. In our case, the agreement between the experimental modulus and theoretical modulus suggested good dispersion and interfacial adhesion between the polymer and VGCNF in the composites with nanofiber loading up to 20 wt%. The lower than predicted tensile properties above 40% VGCNF loading could be attributed to the increasing void content in the composite with increasing VGCNF.

The electrical conductivity data are shown in Fig. 4. The inset of Fig. 4 is the plot of conductivity as a function of nanofiber volume fraction (V), from which a percolation volume (V_c) of 3.1 vol% was obtained. Plotting electrical conductivity as a function of ($V-V_c$) (both axes in logarithmic scales) results in a slope of 1.29, suggesting two-dimensional electrical percolation behavior.

The storage modulus (Fig. 5, top) increased with the VGCNF loading up to 40 wt%. Enhancement in storage modulus was particularly evident above the glass transition temperature. The magnitude of the Tan δ peak decreased (Fig. 5, bottom) with the addition of VGCNF. The tan δ

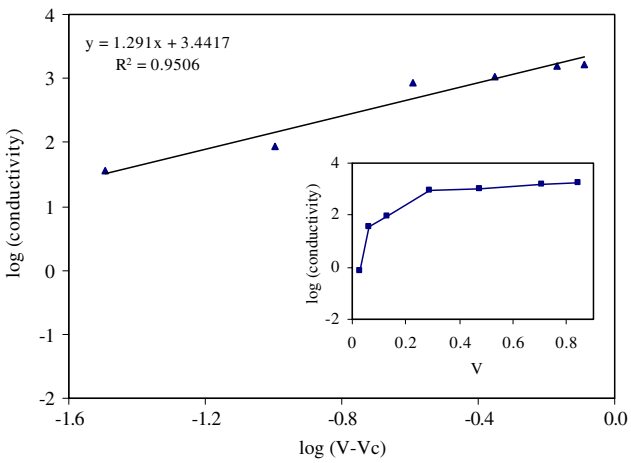

Fig. 4 Electrical conductivity of PAN/VGCNF composite films

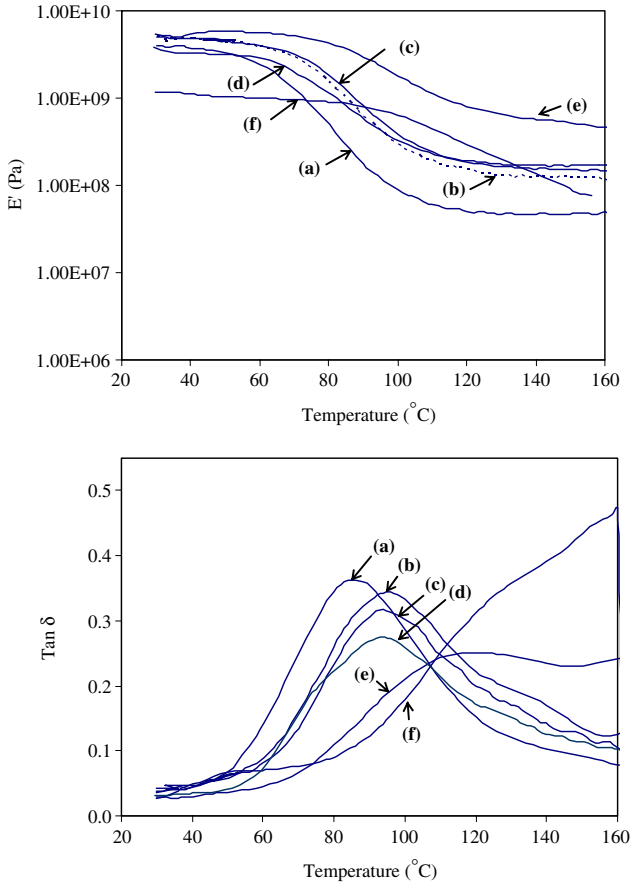

Fig. 5 Storage modulus (top) and Tan δ (below) as a function of temperature for (**a**) Control PAN, (**b**) PAN/5%VGCNF, (**c**) PAN/10%VGNCF, (**d**) PAN/20%VGCNF, (**e**) PAN/40%VGCNF, and (**f**) PAN/90%VGCNF composite films

peak shifts to higher temperatures and broadens toward higher temperatures with the addition of VGCNF. This behavior is similar to the behavior of PAN/single wall carbon nanotube composite [34]. In general, peak broadening increased with increasing amount of nanofiber in the composite except for 20% VGCNF. This observation could be explained in terms of restricted-mobility interphase present in the composite. With increasing amount of nanofiber, the fraction of polymer present at the polymer–nanofiber interphase increases. As stated previously, significant amount of this polymer at the interphase becomes immobilized, hence resulting in tan δ peak broadening. This effect was very pronounced at nanofiber loading higher than 40% (Fig. 5).

Figure 6 gives the Tan δ peak as a function of temperature for PAN and PAN/VGCNF composite films at various frequencies. The tan δ peak temperatures at various frequencies are listed in Table 4. The activation energy for the PAN molecular motion was calculated using Arrhenius equation:

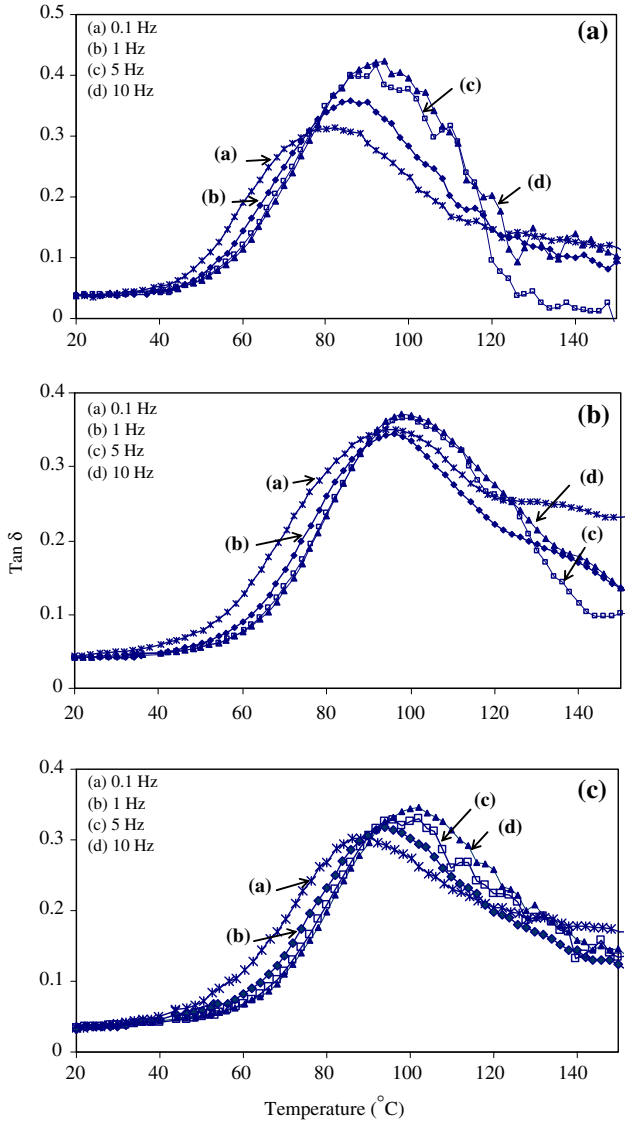

Fig. 6 Tan δ behavior of (**A**) Control PAN, (**B**) PAN/VGCNF (95/5), and (**C**) PAN/VGCNF (90/10) films as a function of temperature at various frequencies

Table 4 Temperature of Tan δ peak at various frequencies

Sample	Temperature (°C)			
Frequency (Hz):	0.1	1	5	10
PAN	82.2	88.0	92.1	94.0
PAN/VGCNF (95/5)	94.1	96.1	100.0	100.2
PAN/VGCNF (90/10)	90.3	93.9	97.6	100.1

$$\mathrm{Ln}\, f = \mathrm{Ln}\, C - E_a/RT \quad (6)$$

where f is the frequency, C is the material constant, E_a is the activation energy, R is the gas constant (8.314 KJ/mole), and T is the absolute temperature. The slope of Ln f versus $1/T$ plot gives the activation energy. The activation

energy for PAN molecular motion in the control PAN film was 425 KJ/mole. For the composite films with 5 and 10 wt% VGCNF loading, the activation energy values were 754 and 535 KJ/mole, respectively. The higher activation energy needed for PAN molecular motion in the composite films indicated interaction between polymer and carbon nanofiber, resulting in hindered motion for polymer molecules. The activation energy for PAN molecular motion was lower for PAN/10% VGCNF composite as compared to PAN/5%VGCNF. We do not fully understand the reasons for decrease in activation energy at 10% VGCNF loading.

Figure 7 shows the wide-angle X-ray diffraction plots of VGCNF, control PAN, and PAN/VGCNF composites. The peak at 43.5° is attributed to the (100) peak in graphite [35]. The crystal size of the graphite (002) plane in the composite film is listed in Table 5. The crystal size of graphite in the composite film with VGCNF loading higher than 20% was almost the same as that in the VGCNF powder. However, the average crystal size of graphite in the composite films with lower VGCNF loading (5 wt% and 10 wt%) was smaller than that in VGCNF powder. PAN and PAN/VGCNF films exhibit a characteristic PAN X-ray diffraction peak at 16.9° attributed to the PAN (110) peak [36]. PAN crystallite size calculated using the Scherrer equation [37] from the (110) peak and PAN crystallinity values are also given in Table 5. At lower VGCNF loading (<20 wt%), PAN crystal size in the composite films was larger than that for the control PAN film. However, for the film with fiber loading with 40 wt% and higher, PAN crystal size decreased with further addition of nanofibers. The percent crystallinity of PAN in the composites did not show any significant trend.

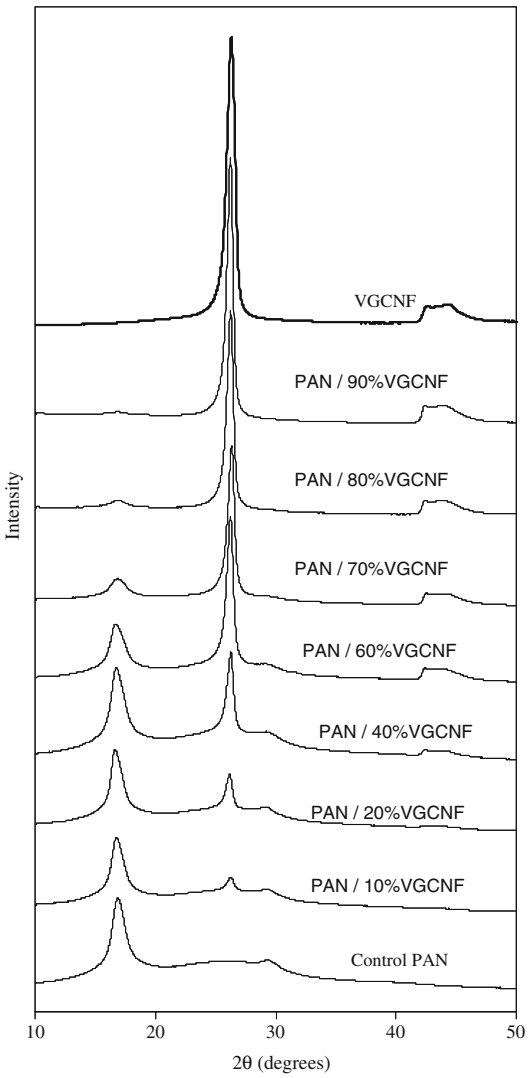

Fig. 7 Wide-angle X-ray diffraction of VGCNF powder, control PAN, and PAN/VGCNF composite films

Scanning electron micrographs for VGCNF and 20 wt% VGCNF films are shown in Fig. 8a and b, respectively. The images reveal a coating of nanofiber by PAN (arrows in 8b) to form a PAN shell and VGCNF core structure. Figure 8c shows the morphology of tensile fracture for PAN/VGCNF film with 5 wt% VGCNF loading. When the composite film was stretched and then broken, a hole was left in the polymer matrix due to slippage of VGCNF from the polymer matrix. PAN was observed in the center of the hole suggesting that some PAN molecules do enter into hollow nanofibers.

Conclusions

PAN/VGCNF composite films with different VGCNF loadings have been processed. The tensile modulus and strength were increased by 20% and 50%, respectively, upon addition of 5 wt% VGCNF. Electrical conductivity of composites increased with the nanofiber loading and exhibited percolation at 3.1 vol%. The storage modulus of PAN was enhanced by incorporation of nanofibers,

Table 5 Wide-angle X-ray diffraction results of VGCNF powder, control PAN, and PAN/VGNF composite films

VGCNF loading (wt%)	Graphite crystal Size (nm)	PAN crystallite size (nm)	PAN crystallinity (%)
0	–	5.7	43
5	12	6.4	46
10	13	6.7	41
20	14	5.9	43
40	14	5.4	40
60	14	4.7	48
80	15	4.3	47
90	16	4.6	43
100	15	–	–

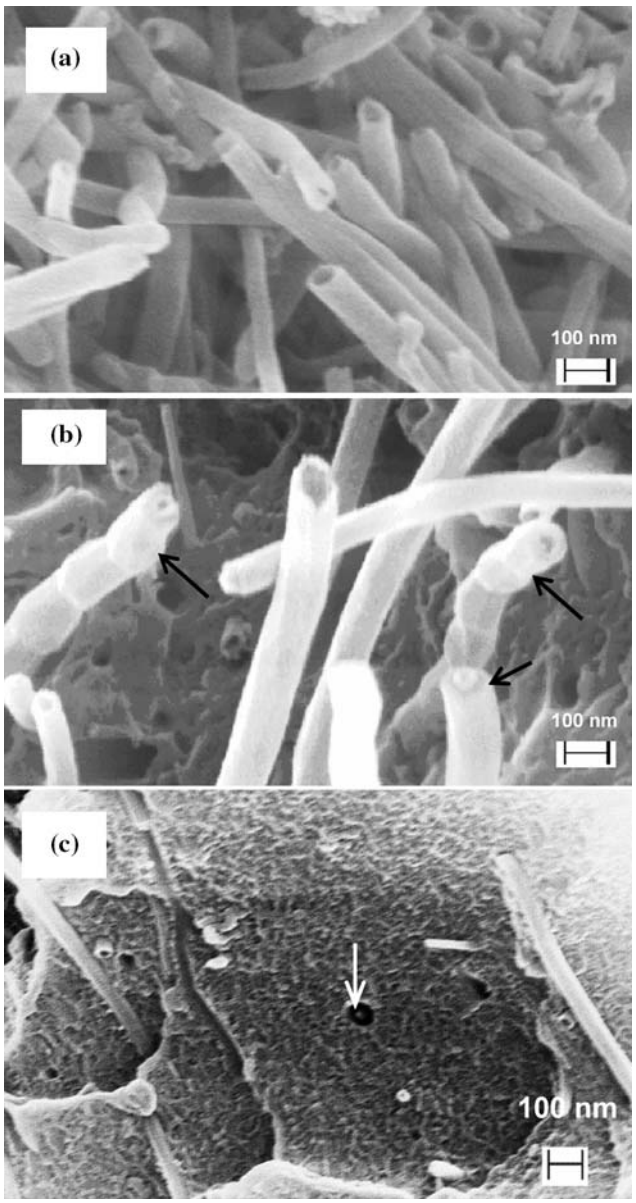

Fig. 8 Scanning electron micrographs for (**a**) VGCNF powder, (**b**) PAN/20%VGCNF, and (**c**) PAN/5%VGCNF composite films

particularly above the glass transition temperature. The tan δ peak broadens and shifts to higher temperatures with the addition of VGCNF. The activation energy needed for PAN molecular motion in the composite films was higher than that in the control PAN film. PAN crystallite size, PAN crystallinity, and graphite crystallite size in various films were calculated and compared. The coating of PAN around the nanofiber was observed. Specific modulus of the composite films containing up to 20% VGCNF was in good agreement with the Halpin-Tsai theory.

Acknowledgements This work was supported by AFOSR (FA9550-06-1-0122 and FA9550-07-1-0233).

References

1. Lake ML, Ting JM (1999) In: Burchell TD (Ed) Carbon materials for advanced technologies. Oxford, UK, pp 139–167
2. De Jong KP, Geus JW (2000) Catal Rev-Sci Eng 42:481
3. Tibbetts GG, Devour MG (1986) U.S. Patent 4,565,684
4. Tibbetts GG (1989) Carbon 27:745
5. Uchida T, Anderson DP, Minus ML, Kumar S (2006) J Mater Sci 41:5851. doi:10.1007/s10853-006-0324-0
6. Choi YK, Gotoh Y, Sugimoto KI, Song SM, Yanagisawa T, Endo M (2005) Polymer 46:11489
7. Patton RD, Pittman CU, Wang L, Hill JR (1999) Compos A-Appl Sci Manuf 30:1081
8. Prasse T, Cavaille JY, Bauhofer W (2003) Compos Sci Technol 63:1835
9. Lozano K, Yang SY, Zeng Q (2004) J Appl Polym Sci 93:155
10. Hine P, Broome V, Ward I (2005) Polymer 46:10936
11. Lozano K, Bonilla-Rios J, Barrera EV (2001) J Appl Polym Sci 80:1162
12. Lozano K, Bonilla-Rios J, Barrera EV (2001) J Appl Polym Sci 80:125
13. Carneiro OS, Maia JM (2000) Polym Compos 21:960
14. Hammel E, Tang X, Trampert M, Schmitt T, Mauthner K, Eder A, Potschke P (2004) Carbon 42:1153
15. Kumar S, Doshi H, Srinivasarao M, Park JO, Schiraldi DA (2002) Polymer 43:1701
16. Caldeira G, Maia JM, Carneiro OS, Covas JA, Bernardo CA (1998) Polym Compos 19:147
17. Carneiro OS, Maia JM (2000) Polym Compos 21:970
18. Carneiro OS, Covas JA, Bernardo CA, Caldeira G, Van Hattum FWJ, Ting JM, Alig RL, Lake ML (1998) Compos Sci Technol 58:401
19. Choi YK, Sugimoto KI, Song SM, Endo M (2005) Mater Lett 59:3514
20. Higgins BA, Brittain WJ (2005) Eur Polym J 41:889
21. Enomoto K, Yasuhara T, Kitakata S, Murakami H, Ohtake N (2004) New Diamond Frontier Carbon Technol 14:11
22. Shofner ML, Lozano K, Rodriguez-Macias FJ, Barrera EV (2003) J Appl Polym Sci 89:3081
23. Tibbetts GG, McHugh JJ (1999) J Mater Res 14:2871
24. Pogue RT, Ye J, Klosterman DA, Glass AS, Chartoff RP (1998) Compos A-Appl Sci Manuf 29:1273
25. Ogasawara T, Ishida Y, Ishikawa T (2004) Adv Compos Mater 13:215
26. Zeng JJ, Saltysiak B, Johnson WS, Schiraldi DA, Kumar S (2004) Compos B-Eng 35:173
27. Ma HM, Zeng JJ, Realff ML, Kumar S, Schiraldi DA (2003) Compos Sci Technol 63:1617
28. Uchida T, Dang T, Min BG, Zhang XF, Kumar S (2005) Compos B-Eng 36:183
29. Chae HG, Sreekumar TV, Uchida T, Kumar S (2005) Polymer 46:10925
30. Oakey J, Marr DWM, Schwartz KB, Wartenberg M (1999) Macromolecules 32:5399
31. Shi DL, Lian J, He P, Wang LM, Xiao F, Yang L, Schulz MJ, Mast DB (2003) Appl Phys Lett 83:5301
32. Mouritz AP (2000) J Compos Mater 34:218
33. Halpin JC, Kardos JL (1976) Polym Eng Sci 16:344
34. Sreekumar TV, Liu T, Min BG, Guo H, Kumar S, Hauge RH, Smalley RE (2004) Adv Mater 16:58
35. Kumar S, Anderson DP, Crasto AS (1993) J Mater Sci 28:423. doi:10.1007/BF00357820
36. Gupta AK, Singhal RP (1983) J Polym Sci B-Polym Phys 21:2243
37. Cullity BD (1978) Elements of X-ray diffraction, 2nd edn. Addison-Wesley, MA, p 102